Physics Letters B 779 (2018) 64–71

Contents lists available at ScienceDirect

Physics Letters B

www.elsevier.com/locate/physletb

Study of the process $e^+e^- \to K^+K^-$ in the center-of-mass energy range 1010–1060 MeV with the CMD-3 detector

E.A. Kozyrev [a,b,*], E.P. Solodov [a,b], R.R. Akhmetshin [a], A.N. Amirkhanov [a,b], A.V. Anisenkov [a,b], V.M. Aulchenko [a,b], V.S. Banzarov [a], N.S. Bashtovoy [a], D.E. Berkaev [a,b], A.E. Bondar [a,b], A.V. Bragin [a], S.I. Eidelman [a,b], D.A. Epifanov [a,b], L.B. Epshteyn [a,b,c], A.L. Erofeev [a,b], G.V. Fedotovich [a,b], S.E. Gayazov [a,b], A.A. Grebenuk [a,b], S.S. Gribanov [a,b], D.N. Grigoriev [a,b,c], F.V. Ignatov [a], V.L. Ivanov [a,b], S.V. Karpov [a], A.S. Kasaev [a], V.F. Kazanin [a,b], A.A. Korobov [a,b], I.A. Koop [a], A.N. Kozyrev [a,b], P.P. Krokovny [a,b], A.E. Kuzmenko [a,b], A.S. Kuzmin [a,b], I.B. Logashenko [a,b], P.A. Lukin [a,b], A.P. Lysenko [a], K.Yu. Mikhailov [a,b], V.S. Okhapkin [a], E.A. Perevedentsev [a,b], Yu.N. Pestov [a], A.S. Popov [a,b], G.P. Razuvaev [a,b], Yu.A. Rogovsky [a,b], A.A. Ruban [a], N.M. Ryskulov [a], A.E. Ryzhenenkov [a,b], V.E. Shebalin [a,b], D.N. Shemyakin [a,b], B.A. Shwartz [a,b], D.B. Shwartz [a,b], A.L. Sibidanov [d], Yu.M. Shatunov [a], A.A. Talyshev [a,b], A.I. Vorobiov [a], Yu.V. Yudin [a,b]

[a] *Budker Institute of Nuclear Physics, SB RAS, Novosibirsk, 630090, Russia*
[b] *Novosibirsk State University, Novosibirsk, 630090, Russia*
[c] *Novosibirsk State Technical University, Novosibirsk, 630092, Russia*
[d] *University of Victoria, Victoria, British Columbia, V8W 3P6, Canada*

ARTICLE INFO

Article history:
Received 10 October 2017
Received in revised form 23 January 2018
Accepted 24 January 2018
Available online 2 February 2018
Editor: L. Rolandi

ABSTRACT

The process $e^+e^- \to K^+K^-$ has been studied using 1.7×10^6 events from a data sample corresponding to an integrated luminosity of 5.7 pb^{-1} collected with the CMD-3 detector in the center-of-mass energy range 1010–1060 MeV. The cross section is measured with about 2% systematic uncertainty and is used to calculate the contribution to the anomalous magnetic moment of the muon $a_\mu^{K^+K^-} = (19.33 \pm 0.40) \times 10^{-10}$, and to obtain the $\phi(1020)$ meson parameters. We consider the relationship between the $e^+e^- \to K^+K^-$ and $e^+e^- \to K_S^0K_L^0$ cross sections and compare it to the theoretical prediction.

1. Introduction

Investigation of e^+e^- annihilation into hadrons at low energies provides unique information about interactions of light quarks. A precise measurement of the $e^+e^- \to K^+K^-$ cross section in the center-of-mass energy range $E_{c.m.} = 1010$–1060 MeV allows to obtain the $\phi(1020)$ meson parameters and to estimate a contribution of other light vector mesons, $\rho(770)$, $\omega(782)$, to this process. The $e^+e^- \to K^+K^-$ cross section, particularly in the ϕ meson energy region, is also required for a precise calculation of the hadronic contribution to the muon anomaly, a_μ, and the value of the fine structure constant at the Z boson peak, $\alpha(M_Z)$ [1].

The most precise cross section measurements performed by the CMD-2 [2] and BaBar [3] experiments have tension at the level of more than 5% (about 2.6 standard deviations) in the ϕ meson energy region.

Another motivation for this study arises from the comparison of the charged $e^+e^- \to K^+K^-$ and neutral $e^+e^- \to K_S^0K_L^0$ final states. A significant deviation of the ratio of the coupling constants $\frac{g_{\phi\to K^+K^-}}{g_{\phi\to K_S^0K_L^0}}$ from a theoretical prediction based on previous experiments (see the discussion in Ref. [4]) requires a new precise measurement of the cross sections.

2. CMD-3 detector and data set

The Cryogenic Magnetic Detector (CMD-3) is a general-purpose detector installed in one of the two interaction regions of the

* Corresponding author.
E-mail address: e.a.kozyrev@inp.nsk.su (E.A. Kozyrev).

https://doi.org/10.1016/j.physletb.2018.01.079

VEPP-2000 collider [5] and is described elsewhere [6]. A detector tracking system consists of a cylindrical drift chamber (DC) and a double-layer cylindrical multiwire proportional chamber (Z-chamber), both installed inside a thin (0.2 X_0) superconducting solenoid with a 1.3 T field. The DC comprises of 1218 hexagonal cells and allows to measure charged particle momentum with a 1.5–4.5% accuracy in the 100–1000 MeV/c momentum range. It also provides a measurement of the polar (θ) and azimuthal (ϕ) angles with an accuracy of 20 mrad and 3.5–8.0 mrad, respectively. Amplitude information from the DC wires is used to measure the ionization losses dE/dx of charged particles with a $\sigma_{dE/dx}/ < \mathrm{dE/dx} > \approx 11$–14% accuracy for minimum ionization particles (m.i.p.). The Z-chamber with cathode strip readout is used to calibrate a DC longitudinal scale.

An electromagnetic calorimeter comprised of a liquid xenon volume of a 5.4 radiation length (X_0) thickness followed by CsI crystals (8.1 X_0) outside of the solenoid in the barrel part and BGO crystals (14.4 X_0) in the end cap parts [7,8]. A flux return yoke of the detector is surrounded by scintillation counters to veto cosmic events.

The beam energy $\mathrm{E_{beam}}$ is monitored by using the back-scattering laser light system [9,10], which determines $\mathrm{E_{c.m.}}$ at each energy point with about 0.06 MeV systematic accuracy.

Candidate events are recorded using signals from two independent trigger systems. One, a charged trigger, uses information only from DC cells indicating the presence of at least one charged track, while the other, a neutral trigger, requires an energy deposition in the calorimeter above $\mathrm{E_{beam}}/2$ or the presence of more than two clusters above 25 MeV threshold.

To study the detector response for the investigated processes and to obtain the detection efficiency, we have developed a Monte Carlo (MC) simulation of the detector based on the GEANT4 [11] package. Simulated events are subject to all reconstruction and selection procedures. MC includes photon jet radiation by initial electron or positron (ISR) calculated according to Ref. [12].

The measurement of the $e^+e^- \to K^+K^-$ cross section presented here is based on a data sample collected at 24 energy points with a 5.7 pb^{-1} integrated luminosity (IL) in the energy range $\mathrm{E_{c.m.}} = 1010$–1060 MeV in 2012 and 2013.

3. Event selection

Selection of $e^+e^- \to K^+K^-$ candidates is based on the detection of two collinear tracks satisfying the following criteria:

- The tracks originate from the beam interaction region within 20 cm along the beam axis (Z-coordinate) and within 1 cm in the transverse direction.
- The polar and azimuthal collinearity are required to have $\Delta\theta = |\theta_{K^+} + \theta_{K^-} - \pi|$, $\Delta\phi = ||\phi_{K^+} - \phi_{K^-}| - \pi| < 0.45$ radians. The distributions of these parameters for data and MC at $\mathrm{E_{beam}} = 530$ MeV are shown in Figs. 1, 2, where the MC sample is normalized to data, and arrows demonstrate the applied requirement. Two additional bumps in the $\Delta\theta$ distribution are caused by a significant contribution of $K^+K^-\gamma$ events, where γ is emitted from the initial state (radiative return to the ϕ resonance).
- The tracks are required to have an average polar angle in the range $1 < \theta_{\mathrm{aver}} = (\theta_{K^+} + \pi - \theta_{K^-})/2 < \pi - 1$ radians. The polar angle distribution is shown in Fig. 3 (top) where arrows show the applied restriction. Tracks outside the selected range do not pass all DC layers and are detected less efficiently (see the discussion in Sec. 6).
- Momenta of both tracks are required to be close to each other: $|p_1 - p_2|/|p_1 + p_2| < 0.3$.

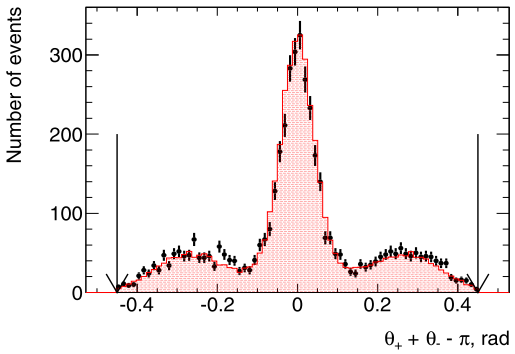

Fig. 1. The polar collinearity $\theta_{K^+} + \theta_{K^-} - \pi$ for data (points) and MC (shaded histogram) at $\mathrm{E_{beam}} = 530$ MeV.

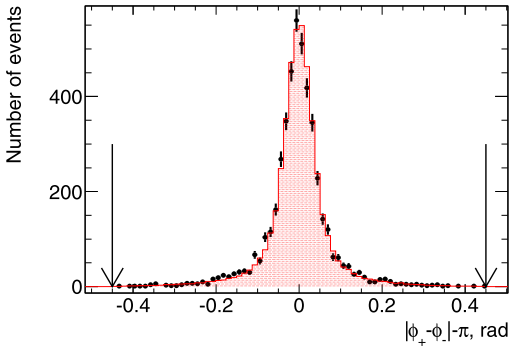

Fig. 2. The azimuthal collinearity $|\phi_{K^+} - \phi_{K^-}| - \pi$ for data (points) and MC (shaded histogram) at $\mathrm{E_{beam}} = 530$ MeV.

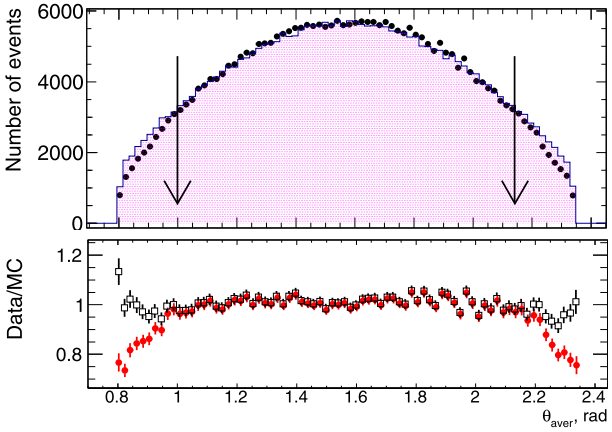

Fig. 3. (top) The average polar angle $\theta_{\mathrm{aver}} = (\theta_{K^+} + \pi - \theta_{K^-})/2$ distribution for data (points) and MC (shaded) at $\mathrm{E_{beam}} = 509.5$ MeV. The MC histogram is normalized to six central bins of the data distribution. (bottom) The data-MC ratio before (points) and after (squares) applying efficiency corrections (see Sec. 6).

- The average momentum of the two tracks is required to be in a range depending on $\mathrm{E_{beam}}$ to minimize the background-to-signal ratio. An example of this restriction for $\mathrm{E_{beam}} = 530$ MeV is shown in Fig. 4 by arrows: the loss of signal events is less than 0.2% according to MC.
- In our energy range kaon ionization losses in the DC are significantly larger than those for m.i.p. due to the low momentum of kaons, $p = 100 \div 200$ MeV/c. We require both tracks to have ionization losses above a value, which is obtained by taking into account the average value of dE/dx at the measured kaon momentum and dE/dx resolution. The line in Fig. 4 shows an example of the applied selection. As seen in the figure, among

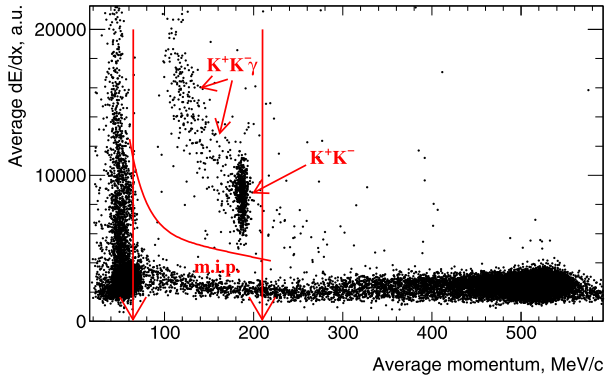

Fig. 4. The ionization losses vs momentum for positive tracks for data at $E_{beam} = 530$ MeV. The lines show the acceptance for the signal region.

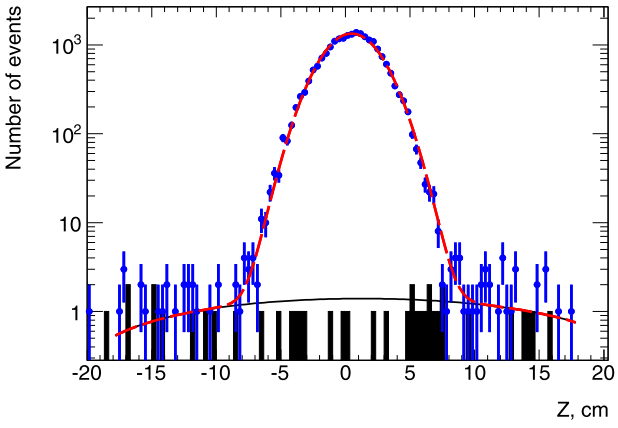

Fig. 5. Distribution of average Z-coordinates of selected tracks at $E_{beam} = 505$ MeV. The long-dotted line corresponds to the signal, the solid line to the background. The shaded histogram shows the background distribution obtained using events at $E_{c.m.} = 984$ MeV.

selected events there are those with ISR photons, which have smaller momentum and therefore larger dE/dx. Such events are also retained for further analysis.

The number of signal events is obtained using a fit of the average Z-coordinate distribution of two selected tracks with signal and background functions shown in Fig. 5. The shape of the signal function is described by a sum of two Gaussian distributions with parameters fixed from the simulation, and with additional Gaussian smearing to account for the difference in data-MC detector responses. For the background profile we use a second-order polynomial function, which describes well a distribution obtained at the energy $E_{c.m.} = 984$ MeV below the threshold of the K^+K^- production shown in Fig. 5 by a shaded histogram. The level of background is estimated to be less than 0.5% for all energy points, except for the lowest energy $E_{c.m.} = 1010.46$ MeV, where the background is about 1.1%. The background is predominantly caused by the beam-gas interaction and interaction of particles lost from the beam at the vacuum pipe walls.

As a result, we obtain 1705060 ± 1306 $e^+e^- \to K^+K^-$ signal events.

4. Detection efficiency

The detection efficiency, ϵ_{MC}, is determined from MC by dividing the number of MC simulated events, after reconstruction and selection described above, to the total number of generated K^+K^- pairs. The obtained ϵ_{MC} is presented in Table 1 from 44% to 55% and is primarily determined by the restriction on the kaon polar angles and its decays in flight. Simulation of the ISR spectrum depends on the cross section under study and this effect is taken into account by iterations. Influence of final-state radiation of real photons (FSR) on ϵ_{MC} is examined by including into the MC generator the FSR amplitude calculated according to scalar electrodynamics with point-like K mesons [12]. The observed change of ϵ_{MC} is less than 0.1%.

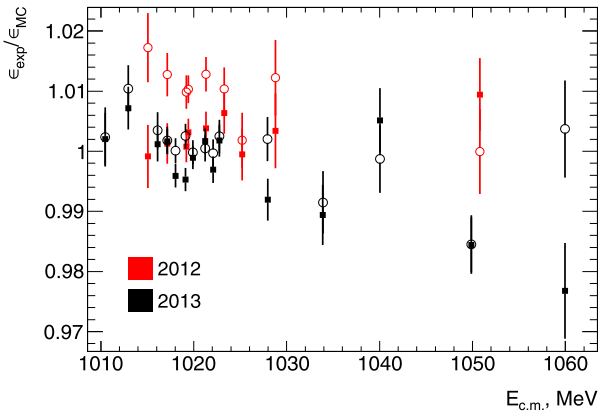

Fig. 6. The EXP-MC ratio of the single-track efficiencies for positive $\frac{\epsilon^+_{EXP}}{\epsilon^+_{MC}}$ (squares) and negative $\frac{\epsilon^-_{EXP}}{\epsilon^-_{MC}}$ (circles) kaons for data collected in 2012 and 2013 runs.

Because of some data-MC inconsistency in the tracking efficiency, we introduce a correction equal to the ratio of a single-kaon track efficiency in data and MC, $\epsilon^{+(-)}_{EXP}/\epsilon^{+(-)}_{MC}$. A detection efficiency corrected for detector effects is defined as

$$\epsilon_{det} = \epsilon_{MC} \frac{\epsilon^+_{EXP}}{\epsilon^+_{MC}} \frac{\epsilon^-_{EXP}}{\epsilon^-_{MC}}. \quad (1)$$

The collinear configuration of the process and large ionization losses allow estimation of the single-kaon track efficiency in data and MC to be performed by selecting a pure class of "test" events with a detected positive or negative charged kaon, and checking how often we reconstruct the opposite track. The detection efficiencies for single positive and negative kaons increase from 80% to 90% in our energy range. The data-MC ratios $\frac{\epsilon^+_{EXP}}{\epsilon^+_{MC}}$ and $\frac{\epsilon^-_{EXP}}{\epsilon^-_{MC}}$ of the single-track efficiencies are shown in Fig. 6 for positive (squares) and negative (circles) charged kaons vs c.m. energy, and are used in Eq. (1) to calculate the detection efficiency for each energy point.

5. Cross section of $e^+e^- \to K^+K^-$

The experimental Born cross section of the process $e^+e^- \to K^+K^-$ has been calculated for each energy point according to the expression:

$$\sigma^{born} = \frac{N_{exp}}{\epsilon_{det} \cdot \epsilon_{trig} \cdot IL \cdot (1+\delta^{rad.})} \cdot (1+\delta^{en.spr.}), \quad (2)$$

where ϵ_{trig} is a trigger efficiency, IL is the integrated luminosity, $1+\delta^{en.spr.}$ represents a correction due to the energy spread of the electron–positron beams, and $1+\delta^{rad.}$ is the initial-state radiative correction. The integrated luminosity IL is determined by the processes $e^+e^- \to e^+e^-$ and $e^+e^- \to \gamma\gamma$ with an about accuracy of about 1% [14,15]. The correction $1+\delta^{rad.}$, shown by squares in Fig. 7, is calculated using the radiative structure function, known with an accuracy better than 0.1% [13].

Table 1
The c.m. energy $E_{\text{c.m.}}$, number of selected signal events N, uncorrected and corrected detection efficiencies ϵ_{MC} and ϵ_{det}, radiative correction factor $1+\delta^{\text{rad.}}$, correction for the spread of collision energy $1+\delta^{\text{en.spr.}}$, integrated luminosity IL, and Born cross section σ for the process $e^+e^- \to K^+K^-$. Only statistical errors are shown.

$E_{\text{c.m.}}$, MeV	N events	ϵ_{MC}	ϵ_{det}	$1+\delta^{\text{rad.}}$	$1+\delta^{\text{en.spr.}}$	IL, nb^{-1}	σ, nb
1010.47 ± 0.01	21351 ± 145	0.439	0.441	0.735	0.993	936.05 ± 1.44	69.87 ± 0.50
1012.96 ± 0.01	26882 ± 164	0.485	0.493	0.728	0.988	485.36 ± 1.04	152.45 ± 1.01
1015.07 ± 0.02	6031 ± 78	0.502	0.510	0.718	0.987	47.91 ± 0.33	341.10 ± 5.11
1016.11 ± 0.01	41260 ± 201	0.510	0.513	0.712	0.978	192.11 ± 0.66	575.08 ± 3.84
1017.15 ± 0.02	176768 ± 421	0.515	0.517	0.706	0.983	478.99 ± 1.04	993.19 ± 5.02
1017.16 ± 0.02	22243 ± 149	0.517	0.524	0.706	0.985	60.15 ± 0.30	984.71 ± 8.89
1018.05 ± 0.03	279733 ± 529	0.521	0.519	0.706	0.993	478.34 ± 1.04	1584.27 ± 11.00
1019.12 ± 0.02	270045 ± 520	0.525	0.524	0.721	1.026	328.62 ± 0.86	2228.59 ± 8.13
1019.21 ± 0.03	44051 ± 209	0.525	0.531	0.724	1.022	52.75 ± 0.34	2230.81 ± 18.14
1019.40 ± 0.04	30539 ± 174	0.526	0.533	0.730	1.024	36.05 ± 0.29	2233.66 ± 22.07
1019.90 ± 0.02	391083 ± 626	0.527	0.527	0.752	1.017	472.34 ± 1.04	2127.07 ± 6.46
1021.22 ± 0.03	134598 ± 365	0.532	0.533	0.829	0.994	228.34 ± 0.72	1325.01 ± 9.01
1021.31 ± 0.01	27717 ± 165	0.531	0.540	0.835	0.993	46.85 ± 0.33	1308.31 ± 12.50
1022.08 ± 0.03	89487 ± 299	0.532	0.530	0.885	0.989	201.62 ± 0.68	933.95 ± 6.81
1022.74 ± 0.03	41756 ± 204	0.534	0.536	0.928	0.988	116.71 ± 0.52	710.23 ± 5.86
1023.26 ± 0.04	19718 ± 140	0.536	0.545	0.961	0.991	62.91 ± 0.38	595.03 ± 6.56
1025.32 ± 0.04	7023 ± 84	0.537	0.538	1.077	0.995	36.32 ± 0.29	334.77 ± 5.55
1027.96 ± 0.02	24236 ± 156	0.540	0.536	1.200	0.997	195.83 ± 0.67	191.64 ± 1.74
1029.09 ± 0.02	5786 ± 76	0.542	0.550	1.244	0.997	52.94 ± 0.35	159.94 ± 2.95
1033.91 ± 0.02	11752 ± 108	0.546	0.535	1.392	0.998	175.55 ± 0.64	89.65 ± 1.24
1040.03 ± 0.05	9143 ± 95	0.551	0.553	1.509	0.999	195.91 ± 0.68	55.87 ± 0.94
1049.86 ± 0.02	14818 ± 122	0.553	0.536	1.604	0.999	499.59 ± 1.09	34.47 ± 0.47
1050.86 ± 0.04	4441 ± 67	0.554	0.559	1.609	0.999	146.31 ± 0.59	33.89 ± 0.84
1059.95 ± 0.02	4594 ± 68	0.553	0.543	1.640	0.999	198.86 ± 0.69	25.93 ± 0.64

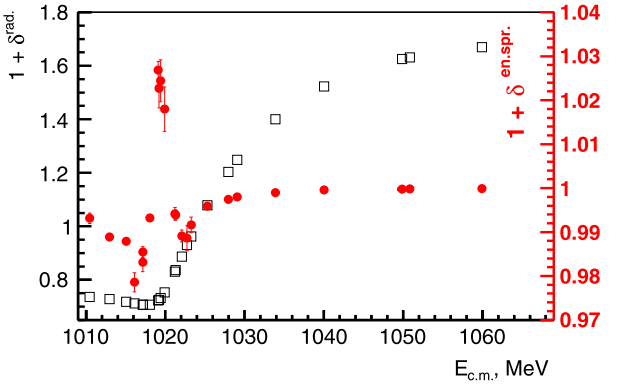

Fig. 7. Radiative correction $1+\delta^{\text{rad.}}$ (squares, left scale) and correction $1+\delta^{\text{en.spr.}}$ for the spread of collision energy (points, right scale).

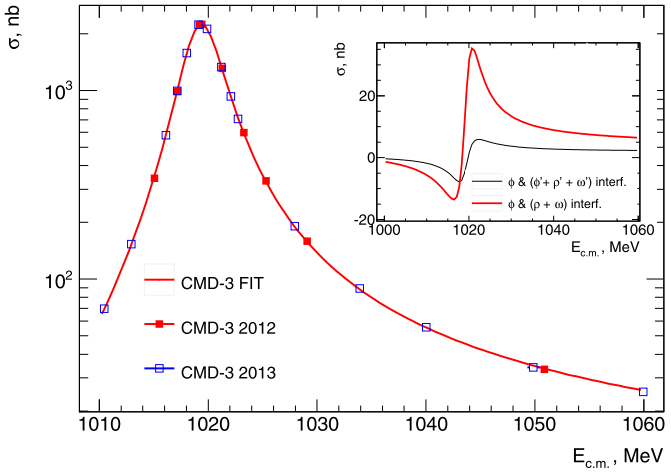

Fig. 8. Measured $e^+e^- \to K^+K^-$ cross section. The dots are experimental data, the curve is the fit described in the text.

The electron–positron c.m. energy spread, $\sigma_{E_{\text{c.m.}}}$, typically about 300 keV, changes the visible cross section. To take into account this effect we apply the following correction:

$$1+\delta^{\text{en.spr.}}(E_{\text{c.m.}}) = \frac{1}{\sqrt{2\pi}\sigma_{E_{\text{c.m.}}}} \cdot \tag{3}$$

$$\cdot \frac{\int dE'_{\text{c.m.}} \sigma^{\text{born}}(E'_{\text{c.m.}})(1+\delta^{\text{rad.}}(E'_{\text{c.m.}}))e^{-\frac{(E'_{\text{c.m.}}-E_{\text{c.m.}})^2}{2\sigma^2_{E_{\text{c.m.}}}}}}{\sigma^{\text{born}}(E_{\text{c.m.}})(1+\delta^{\text{rad.}}(E_{\text{c.m.}}))},$$

which depends on the cross section σ^{born}, radiative correction $(1+\delta^{\text{rad.}})$, and is calculated by iterations in the same way as ϵ_{MC} and $(1+\delta^{\text{rad.}})$. The calculated $(1+\delta^{\text{en.spr.}})$ value for each energy point is shown in Fig. 7 by circles (right scale), and has the maximum value of 1.026 ± 0.006 at the peak of the ϕ resonance.

The trigger efficiency, ϵ_{trig}, is studied using responses of two independent charged and neutral triggers, for selected signal events, and is found to be close to 100% for the applied selection.

The resulting cross section is listed for each energy point in Table 1 and shown in Fig. 8. The statistical error includes fluctuations of signal and Bhabha events, used for the luminosity calculation, and fluctuations of the uncertainty on the c.m. energy measurement, $\delta E_{\text{c.m.}}$, calculated as $|\frac{\partial\sigma^{\text{born}}}{\partial E_{\text{c.m.}}}| \times \delta E_{\text{c.m.}}$.

6. Systematic uncertainties

The uncertainty on the $e^+e^- \to K^+K^-$ cross section is dominated by the accuracy on the determination of the detection efficiency ϵ_{det}.

The systematic uncertainty of the data-MC ratios in Eq. (1) is estimated by applying different selection requirements on the "test" events and does not exceed 1%. However, for five energy points with $E_{\text{c.m.}} > 1030$ MeV the uncertainty reaches 2%.

The data-MC difference in the polar angle distributions of kaons is shown in Fig. 3(bottom) by circles. The observed difference is due to incorrect simulation of detector resolution, angular dependence of the track reconstruction and trigger efficiency, and uncertainty on the calibration of the DC longitudinal scale. We tune our simulation to match the detector angular and momentum resolutions (see Fig. 1), to study angular dependence of the track

Table 2
Summary of systematic uncertainties on the $e^+e^- \to K^+K^-$ cross section measurement.

Source	Uncertainty, %
Signal selection	0.3
Detection efficiency	1.6(2.5)
Radiative correction	0.15(0.80)
Energy spread correction	0.3
Trigger efficiency	0.1
Luminosity	1.0
Total	2.0(2.8)

reconstruction efficiency using a single-track test sample, and the response of two independent triggers as a function of the track polar angle. The data-MC ratio of the polar angle distributions after applying corrections is shown in Fig. 3(bottom) by squares.

To estimate the influence of the remaining angular uncertainty on the measured cross section we divide all data into three independent samples with $\theta_{\rm aver} \in [0.95 : 1.35]$, $[1.35 : \pi - 1.35]$ and $[\pi - 1.35 : \pi - 0.95]$ radians. By separately calculating all parameters in Eq. (2) for three regions and comparing the obtained cross sections we estimate the corresponding uncertainty as the average difference of the samples to be 1%.

To check the quality of the DC scale calibration we extrapolate the reconstructed kaon tracks from DC to ZC and compare it with the position of the ZC response: a possible systematic uncertainty is less than 0.3%.

The total systematic uncertainty in the reconstruction efficiency is estimated as 1.6%, but increased to 2.5% for the five energy points with $E_{\rm c.m.} > 1030$ MeV.

To estimate the uncertainty on the background subtraction procedure we use the data accumulated at the energy point $E_{\rm c.m.} = 984$ MeV below the reaction threshold. Applying our selection criteria we obtain the number of background events, N_{984}. Then estimate the number of background events for each energy point using the integrated luminosities $IL(E_{\rm c.m.})$ as:

$$N_{\rm bkg}(E_{\rm c.m.}) = N_{984} \cdot \frac{IL(E_{\rm c.m.})}{IL(984)}. \quad (4)$$

The difference between the expected number of background events and the one obtained by the approximation of the Z-coordinate distribution (see Sec. 3) gives less than 0.3% uncertainty of the cross section: this value is used as an estimate of the corresponding systematic uncertainty.

A significant part of selected signal events includes ISR photons, which should be taken into account in the determination of $\epsilon_{\rm det}$ and $1+\delta^{\rm rad.}$. The photon spectrum is calculated by a convolution of the radiator function [13] and Born cross section $\sigma^{\rm born}(E_{\rm c.m.})$ which is known with uncertainties discussed above. By varying $\sigma^{\rm born}(E_{\rm c.m.})$ according to its systematic uncertainty and repeating the calculation of the values of $(1+\delta^{\rm rad.})$ we estimate the uncertainty on the last ones as 0.1% (0.8% for energy points with $E_{\rm c.m.} > 1030$ MeV). These values are added quadratically with the 0.1% theoretical uncertainty of the radiator function.

The systematic uncertainties contributing to the measured cross section are listed in Table 2, and the quadratic sum gives a total systematic uncertainty of 2.0% (2.8% for $E_{\rm c.m.} > 1030$ MeV).

7. Approximation of the $e^+e^- \to K^+K^-$ cross section

The measured cross section defined by Eq. (2) includes a vacuum polarization factor, Coulomb interaction between K^+K^-, and final-state radiation of real photons γ_{FSR}. We approximate the energy dependence of the cross section according to the vector meson dominance (VMD) model as a squared sum of the ρ, ω, ϕ-like amplitudes [18]:

$$\sigma(s) \equiv \sigma_{e^+e^-\to K^+K^-}(s) = \frac{8\pi\alpha}{3s^{5/2}} p_K^3 \frac{Z(s)}{Z(m_\phi^2)} \left| \frac{g_{\phi\gamma} g_{\phi KK}}{D_\phi(s)} + r_{\rho,\omega} \times \left[\frac{g_{\rho\gamma} g_{\rho KK}}{D_\rho(s)} + \frac{g_{\omega\gamma} g_{\omega KK}}{D_\omega(s)} \right] + A_{\phi',\rho',\omega'} \right|^2, \quad (5)$$

where $s = E^2_{\rm c.m.}$, p_K is the kaon momentum,

$$Z(s) = \frac{\pi\alpha/\beta}{1 - exp(-\pi\alpha/\beta)} \left(1 + \frac{\alpha^2}{4\beta^2}\right) \quad (6)$$

is the Sommerfeld–Gamov–Sakharov factor that can be obtained by solving the Schrödinger equation in a Coulomb potential for a P-wave final state with velocity $\beta = \sqrt{1 - 4m_K^2/s}$, and $D_V(s)$ is the inverse propagator of the vector state V:

$$D_V(s) = m_V^2 - s - i\sqrt{s}\Gamma_V(s). \quad (7)$$

Here m_V and Γ_V are mass and width of the major intermediate resonances: $V = \rho(770)$, $\omega(782)$, $\phi(1020)$. For the energy dependence of the ϕ meson width we use

$$\Gamma_\phi(s) = \Gamma_\phi \cdot \left(B_{K^+K^-} \frac{m_\phi^2 F_{K^+K^-}(s)}{s F_{K^+K^-}(m_\phi^2)} + B_{K_S^0 K_L^0} \frac{m_\phi^2 F_{K_S^0 K_L^0}(s)}{s F_{K_S^0 K_L^0}(m_\phi^2)} + B_{\pi^+\pi^-\pi^0} \frac{\sqrt{s} F_{\pi^+\pi^-\pi^0}(s)}{m_\phi F_{\pi^+\pi^-\pi^0}(m_\phi^2)} + B_{\eta\gamma} \frac{F_{\eta\gamma}(s)}{F_{\eta\gamma}(m_\phi^2)} \right),$$

where $F_{K\bar{K}} = (s/4 - m_K^2)^{3/2}$, $F_{\eta\gamma}(s) = (\sqrt{s}(1 - m_\eta^2/s))^3$. For the $F_{\pi^+\pi^-\pi^0}(s)$ calculation the model assuming the $\phi \to \rho\pi \to \pi^+\pi^-\pi^0$ decay is used [19]. The magnitudes of $\Gamma_\rho(s)$ and $\Gamma_\omega(s)$ are calculated in the same way using the corresponding branching fractions [20]. The coupling constants of the intermediate vector meson V with initial and final states are given by:

$$g_{V\gamma} = \sqrt{\frac{3m_V^3 \Gamma_{Vee}}{4\pi\alpha}}; \; g_{VK^+K^-} = \sqrt{\frac{6\pi m_V^2 \Gamma_V B_{VK^+K^-}}{p_K^3(m_V)}},$$

where Γ_{Vee} and $B_{VK^+K^-}$ are the electronic width and the decay branching fraction to a kaon pair. In our approximation we use the PDG values for the mass, total width, and electronic width of the $\rho(770)$ and $\omega(782)$: $\Gamma_{\rho\to ee} = 7.04 \pm 0.06$ keV, $\Gamma_{\omega\to ee} = 0.60 \pm 0.02$ keV [20]. For the *a priori* unknown couplings of the $\rho(770)$ and $\omega(782)$ to the pair of kaons we use the relation

$$g_{\omega K^+K^-} = g_{\rho K^+K^-} = -g_{\phi K^+K^-}/\sqrt{2}, \quad (8)$$

based on the quark model with "ideal" mixing and exact SU(3) symmetry of u-, d-, and s-quarks [18]. In order to take into account a possible breaking of these assumptions, both $g_{\rho K^+K^-}$ and $g_{\omega K^+K^-}$ are multiplied by a common complex constant $r_{\rho/\omega}$.

The amplitude $A_{\phi',\rho',\omega'}$ denotes a contribution of the higher vector mesons $\omega(1420)$, $\rho(1450)$, $\omega(1650)$, $\phi(1680)$ and $\rho(1700)$ to the $\phi(1020)$ mass region. Using BaBar [3] and SND [16] data above $\sqrt{s} = 1.06$ GeV for the process $e^+e^- \to K^+K^-$ we extract a contribution of these states.

We perform a fit to the $e^+e^- \to K^+K^-$ cross section with free m_ϕ, Γ_ϕ, $\Gamma_{\phi\to ee} \times B_{\phi\to K^+K^-}$ (or alternatively $B_{\phi\to ee} \times B_{\phi\to K^+K^-}$)

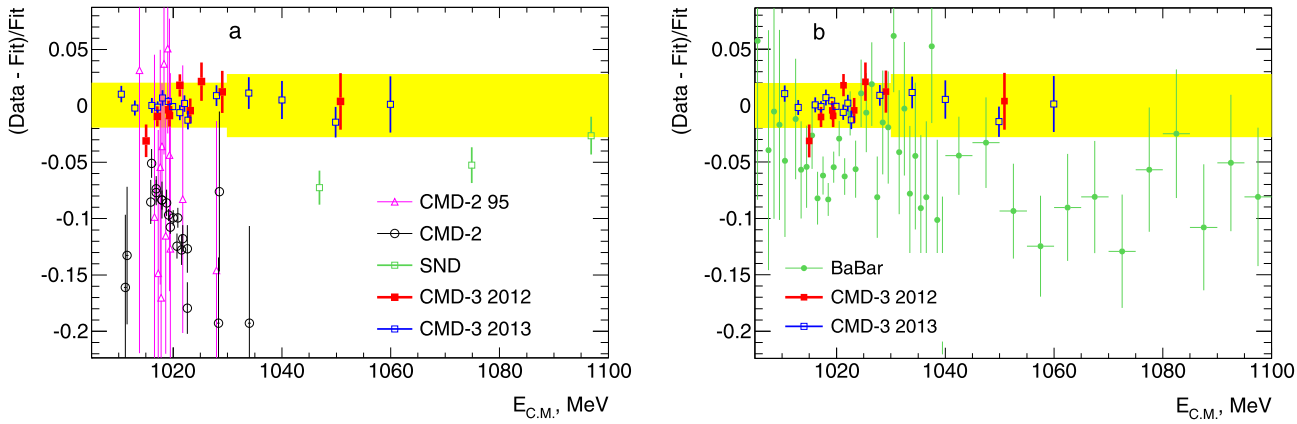

Fig. 9. Comparison of the measured cross section with other experimental data. Only statistical uncertainties are included in data. The width of the band shows the systematic uncertainties.

Table 3
The parameters obtained from a fit of the cross section compared with previous experiments.

Parameter	CMD-3	Other measurements
m_ϕ, MeV	$1019.469 \pm 0.006 \pm 0.060 \pm 0.010$	1019.461 ± 0.019 (PDG2016)
Γ_ϕ, MeV	$4.249 \pm 0.010 \pm 0.005 \pm 0.010$	4.266 ± 0.031 (PDG2016)
$\Gamma_{\phi\to ee}B_{\phi\to K^+K^-}$, keV	$0.669 \pm 0.001 \pm 0.022 \pm 0.005$	0.634 ± 0.008 (BaBar)
$B_{\phi\to ee}B_{\phi\to K^+K^-}$, 10^{-5}	$15.789 \pm 0.033 \pm 0.527 \pm 0.120$	14.24 ± 0.30 (PDG2016)

and $r_{\rho/\omega}$ parameters: the fit yields $\chi^2/ndf = 25/20$ ($P(\chi^2) = 20\%$). The fit result is shown in Fig. 8. Fig. 9 shows the relative difference between the obtained data and the fitted curve. Only statistical errors are shown and the width of the band corresponds to the systematic uncertainty on the cross section. In Fig. 9 (a) we compare our result with previous Novosibirsk measurements [2,16,17] while Fig. 9 (b) shows a comparison with the recent BaBar data [3]. The obtained parameters of the ϕ meson in comparison with the values of other measurements are presented in Table 3. The first uncertainties are statistical and the second are systematic, resulting from the 60 keV accuracy in the $E_{c.m.}$ measurements and errors listed in Table 2. From the fit we obtain Re $(r_{\rho/\omega}) = 0.95 \pm 0.03$ with an imaginary part compatible with zero. The contributions of the ρ and ω intermediate states $(\sigma(s) - \sigma(s)|_{r_{\rho,\omega}=0})$ and higher excitations $(\sigma(s) - \sigma(s)|_{A_{\phi',\rho',\omega'}=0})$ are shown in Fig. 8 as an inset.

To study model dependence of the results, we perform alternative fits with the $A_{\phi',\rho',\omega'} = 0$ amplitude in Eq. (5), or with an additional floating phase of the ϕ meson amplitude, or with the form of the inverse propagator $D_V(s) = m_V^2 - s - im_V\Gamma_V(s)$ instead of Eq. (7). The variations of the ϕ meson parameters in these fits are used as an estimate of the model-dependent uncertainty presented as third errors in Table 3.

As shown in Fig. 9, the obtained results have comparable accuracy but are not consistent, in general, with previous data.

The difference with the CMD-2 [2] measurement can be explained by the overestimation of the value of the trigger efficiency for slow kaons in the previous data. The positive trigger decision from CMD-2 required the presence of one charged track in DC in coincidence with the corresponding hits in the Z-chamber, and with at least one cluster in the CsI calorimeter with an energy deposition greater than 20 MeV. But slow kaons stop in the first wall of the Z-chamber and only decay or their nuclear interaction products can make hits in the Z-chamber or leave energy in the calorimeter. The trigger efficiency of about 90% was obtained actually by simulation, using recorded information from detector cells.

In contrast to CMD-2, the new CMD-3 detector has two independent trigger systems, the Z-chamber is excluded from the decision, and a charged (total) trigger efficiency is close to 100%. The CMD-3 detector has the same Z-chamber with much more detailed information, and by including in our selection requirements of hits in the Z-chamber and the presence of an energy deposition greater than 20 MeV in the barrel calorimeter, we obtain a significantly larger trigger efficiency correction than the value obtained in the CMD-2 analysis [2]. A reanalysis of CMD-2 data is expected.

Our value of $\Gamma_{\phi\to ee}B_{\phi\to K^+K^-}$ is larger than the BaBar result by 1.8 standard deviations while the corresponding value of $B_{\phi\to ee}B_{\phi\to K^+K^-}$ is larger than the PDG one, predominantly based on the CMD-2 measurement, by 2.7 standard deviations. The obtained values of the ϕ meson mass and width agree with the results of other experiments including our recent study of the process $e^+e^- \to K_S^0K_L^0$ [21].

8. Contribution to a_μ

Using the result for the $e^+e^- \to K^+K^-$ cross section we compute the contribution of this channel to the muon anomaly a_μ via a dispersion relation in the energy region $2m_K < E_{c.m.} < 1.06$ GeV. According to Ref. [1], for the leading-order hadronic contribution we obtain:

$$a_\mu^{K^+K^-} = \left(\frac{\alpha m_\mu}{3\pi}\right)^2 \int\limits_{4m_K^2}^{(1.06\ \mathrm{GeV})^2} \frac{ds}{s^2} K(s) \times$$

$$\times \frac{\sigma(e^+e^- \to K^+K^-) \cdot |1 - \Pi(s)|^2}{\sigma_0(e^+e^- \to \mu^+\mu^-)} =$$

$$= (19.33 \pm 0.04_{\mathrm{stat}} \pm 0.40_{\mathrm{syst}} \pm 0.04_{\mathrm{VP}}) \times 10^{-10}, \qquad (9)$$

where $K(s)$ is the kernel function, the factor $|1 - \Pi(s)|^2$ excludes the effect of leptonic and hadronic vacuum polarization (VP), and $\sigma_0(e^+e^- \to \mu^+\mu^-) = \frac{4\pi\alpha^2}{3s}$ is the Born cross section. The first uncertainty is statistical, the second one corresponds to the systematic uncertainty of $\sigma(e^+e^- \to K^+K^-)$ and the third one is the uncertainty of the VP factor (0.2% [23]). In Eq. (9) we integrate the

cross section which includes FSR using the model obtained in the previous section. Then, in order to avoid a model uncertainty, the difference between values of the experimental cross section and the model used, is integrated using the trapezoidal method.

The value should be compared with the recent result of the BaBar collaboration $a_\mu^{K^+K^-} = (18.64 \pm 0.16_{\rm stat} \pm 0.13_{\rm syst} \pm 0.03_{\rm VP}) \times 10^{-10}$ calculated in the same energy range [3]. The difference between the two values is 1.6σ.

9. Comparison of $e^+e^- \to K^+K^-$ and $e^+e^- \to K^0_S K^0_L$ processes

There is a strong relationship between the processes of electron–positron annihilation into K^+K^- and $K^0_S K^0_L$ final states. The difference between them comes from the kinematic effect of the $K^\pm$ and K^0 mass difference and the Coulomb interaction between K^+ and K^- mesons (Eq. (6)). At the ϕ peak, the Coulomb factor, $Z(m_\phi^2)$, contributes 4.2% to the total cross section. We correct the $e^+e^- \to K^+K^-$ cross section for the above two effects and calculate the difference with the $e^+e^- \to K^0_S K^0_L$ cross section:

$$D_{c/n} = \sigma_{e^+e^-\to K^+K^-} \times \frac{\beta^3_{K^0}(s)}{\beta^3_{K^\pm}(s)} \times \frac{1}{Z(s)} - \\ -\delta_{K^0_S K^0_L} \times \sigma_{e^+e^-\to K^0_S K^0_L}, \quad (10)$$

where the factor $\delta_{K^0_S K^0_L}$ is introduced to account for a possible remaining systematic uncertainty in two measurements: most of the common uncertainties cancel in the difference. The experimental value of $D_{c/n}$ is shown in Fig. 10 by points with error bars, where the cross section of the production of neutral kaons is taken from our recent measurement [21]. The shaded area in the figure corresponds to the systematic uncertainties.

The deviation of $D_{c/n}$ from zero mostly comes from the different structure of the amplitudes of non-resonant isovector states, dominated by the ρ meson, for the processes with charged and neutral kaons. Indeed, instead of relations in Eq. (8) for the charged final state, the coupling constants of the $\omega(782)$ and $\rho(770)$ with the $K^0_S K^0_L$ final state are:

$$g_{\omega K^0_S K^0_L} = -g_{\rho K^0_S K^0_L} = -g_{\phi K^0_S K^0_L}/\sqrt{2}, \quad (11)$$

where the ρ-meson term has a different sign. So, the magnitude of $D_{c/n}$ in Eq. (10) is proportional to $\frac{g_{\rho KK} g_{\phi KK}}{D_\phi(s) D_\rho(s)}$, that allows to see experimentally the ρ meson contribution to K-meson production.

We fit $D_{c/n}$ using Eqs. (5), (10) with two free parameters, $r_{\rho/\omega}$ and $\delta_{K^0_S K^0_L}$, discussed above. The mass, width of the ϕ meson and $\Gamma_{\phi\to ee} B_{\phi\to K^+K^-}$ are fixed at the values obtained in Sec. 7, also $\Gamma_{\phi\to ee} B_{\phi\to K^0_S K^0_L}$ is fixed at 0.428 keV according to Ref. [21]. The fit result is shown by a solid line in Fig. 10(a) and, in more detail, in insets to Fig. 10 (b, c) and yields:

$$r_{\rho/\omega} = 0.954 \pm 0.027,$$
$$\delta_{K^0_S K^0_L} = 0.9964 \pm 0.0014,$$
$$\chi^2/ndf = 22.2/22.$$

We obtain good description of data by the fit. A small deviation of $r_{\rho/\omega}$ from unity demonstrates the accuracy ($\approx 5\%$) of relations (8), (11) and confirms that the contribution from the $\rho(770)$ meson to $D_{c/n}$ dominates in the energy range under study. The deviation of $\delta_{K^0_S K^0_L}$ from unity (0.36%) shows the level of a possible remaining systematic uncertainty of the cross section measurements.

Additionally, from the comparison of the charged and neutral cross sections we can obtain the ratio of the coupling constants:

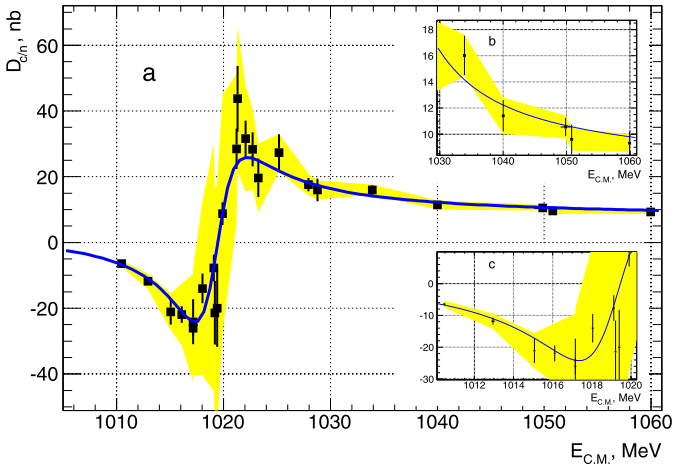

Fig. 10. The difference of the charged and neutral cross sections defined as $D_{c/n} = \sigma_{e^+e^-\to K^+K^-} \times \frac{\beta^3_{K^0}(s)}{\beta^3_{K^\pm}(s)} \times \frac{1}{Z(s)} - \delta_{K^0_S K^0_L} \times \sigma_{e^+e^-\to K^0_S K^0_L}$. The shaded area corresponds to systematic uncertainties in data, the solid line to the fit described in the text.

$$R = \frac{g_{\phi K^+K^-}}{g_{\phi K^0_S K^0_L}\sqrt{Z(m_\phi^2)}} \\ = \sqrt{\frac{B(\phi\to K^+K^-)}{B(\phi\to K^0_S K^0_L)} \cdot \frac{1}{Z(m_\phi^2)} \cdot \frac{\beta^3_{K^0}}{\beta^3_{K^\pm}}} = 0.990 \pm 0.017,$$

where the common parts of systematic uncertainties originating from luminosity, radiative and energy spread corrections, are also reduced. As expected from isospin symmetry of u- and d-quarks, the value of R is consistent with unity.

Additionally to the Coulomb interaction taken into account by the factor $Z(s)$, the final-state radiation of real photons, according to Ref. [22], decreases the total $e^+e^- \to K^+K^-(\gamma)$ cross section by about 0.4% at the ϕ meson mass. This effect partially explains the deviation of R from unity.

10. Conclusion

Using CMD-3 data in the $E_{c.m.} = 1010$–1060 MeV energy range we select 1.7×10^6 events of the process $e^+e^- \to K^+K^-$, and measure the cross section with a systematic error of about 2%. By a fit of the cross section in the VMD model the following values of the ϕ meson parameters have been obtained:

$$m_\phi = 1019.469 \pm 0.061 \text{ MeV}/c^2$$
$$\Gamma_\phi = 4.249 \pm 0.015 \text{ MeV}$$
$$\Gamma_{\phi\to ee} B_{\phi\to K^+K^-} = 0.669 \pm 0.023 \text{ keV}$$

We calculate the contribution of the obtained cross section to the anomalous magnetic moment of the muon $a_\mu^{K^+K^-} = (19.33 \pm 0.40) \times 10^{-10}$ in the energy range from threshold to $\sqrt{s} = 1.06$ GeV.

The observed deviation of the $\rho(770)$ and $\omega(782)$ amplitudes, $r_{\rho/\omega} = 0.95 \pm 0.03$, from a naive theoretical prediction, allows to estimate the accuracy of the used VMD-based phenomenological model to better than 5%. The obtained ratio $\frac{g_{\phi K^+K^-}}{g_{\phi K^0_S K^0_L}\sqrt{Z(m_\phi^2)}} = 0.990 \pm 0.017$ is consistent with isospin symmetry.

Acknowledgements

We thank the VEPP-2000 personnel for the excellent machine operation. This work is supported in part by the Russian Education and Science Ministry, and by the Russian Foundation for Basic Research grants RFBR 15-02-05674, 17-02-00897, 17-52-50064.

References

[1] S. Eidelman, F. Jegerlehner, Z. Phys. C 67 (1995) 585.
[2] R.R. Akhmetshin, et al., Phys. Lett. B 669 (2008) 217.
[3] J.P. Lees, et al., Phys. Rev. D 88 (2013) 032013.
[4] A. Bramon, et al., Phys. Lett. B 486 (2000) 406.
[5] P.Yu. Shatunov, et al., Phys. Part. Nucl. Lett. 13 (2016) 7.
[6] B.I. Khazin, et al., Nucl. Phys. B, Proc. Suppl. 181 (2008) 376.
[7] V.E. Shebalin, et al., Nucl. Instrum. Methods Phys. Res., Sect. A, Accel. Spectrom. Detect. Assoc. Equip. 824 (2016) 710.
[8] V.M. Aulchenko, et al., J. Instrum. 10 (2015) P10006.
[9] E.V. Abakumova, et al., Phys. Rev. Lett. 110 (2013) 140402.
[10] E.V. Abakumova, et al., J. Instrum. 10 (2015) T09001.
[11] S. Agostinelli, et al., GEANT4 Collaboration, Nucl. Instrum. Methods A 506 (2003) 250.
[12] A.B. Arbuzov, et al., Eur. Phys. J. C 46 (2006) 689.
[13] E.A. Kuraev, V.S. Fadin, Sov. J. Nucl. Phys. 41 (1985) 466;
E.A. Kuraev, V.S. Fadin, Yad. Fiz. 41 (1985) 733.
[14] R.R. Akhmetshin, et al., J. Instrum. 9 (2014) C09003.
[15] A.E. Ryzhenenkov, et al., J. Instrum. 12 (2017) C07040.
[16] M.N. Achasov, et al., Phys. Rev. D 94 (2016) 112006.
[17] R.R. Akhmetshin, et al., Phys. Lett. B 364 (1995) 199.
[18] C. Bruch, A. Khodjamirian, J. Kuhn, Eur. Phys. J. C 39 (2005) 41.
[19] N.N. Achasov, et al., Sov. J. Nucl. Phys. 54 (1991) 664;
N.N. Achasov, et al., Yad. Fiz. 54 (1991) 1097;
N.N. Achasov, et al., Int. J. Mod. Phys. A 7 (1992) 3187.
[20] C. Patrignani, et al., Particle Data Group, Chin. Phys. C 40 (2016) 100001.
[21] E.A. Kozyrev, et al., Phys. Lett. B 760 (2016) 314.
[22] A. Hoefer, J. Gluza, F. Jegerlehner, Eur. Phys. J. C 24 (2002) 51.
[23] S. Actis, et al., Eur. Phys. J. C 66 (2010) 585.